Journal of CO2 Utilization 108 (2026) 103467

Contents lists available at ScienceDirect

Journal of CO2 Utilization

journal homepage: www.elsevier.com/locate/jcou

The impact of pressure induced flow instability on gas dispersion in porous media

Tri Pham [a], Rouhi Farajzadeh [b,c], Quoc P. Nguyen [a,*]

[a] Hildebrand Department of Petroleum and Geosystem Engineering, The University of Texas at Austin, Austin, USA
[b] Faculty of Civil Engineering and Geosciences, Delft University of Technology, Delft 2628 CD, the Netherlands
[c] Shell Global Solutions International B.V., The Hague 2596 HP, the Netherlands

ARTICLE INFO

Keywords:
Gas dispersion
Carbonate
Dolomite
Rock heterogeneity
Flow instability

ABSTRACT

Dispersion is influenced by the complex interplay between rock heterogeneity, flow dynamics, and thermodynamic conditions. Previous studies have shown that factors like heterogeneity and injection rate affect how fluids mix and spread in geological formations. However, the role of system pressure and flow regime in shaping dispersion characteristics, particularly under unstable flow conditions, remains less understood. This study examines the effects of system pressure and flow rate on the dispersion of CO_2 and CH_4 in Indiana limestone and Silurian dolomite, two carbonate rocks with distinct pore structures. Experiments were conducted at pressures of 300, 600, and 900 psi, with flow rates of 1.69×10^{-4} m/s, 2.12×10^{-4} m/s, and 3.39×10^{-4} m/s, to evaluate how dispersion characteristics evolve under varying conditions. The results indicate that under stable flow, pressure has minimal impact on dispersion. However, under unstable flow, increasing pressure alters velocity distributions and enhances fluid mixing, leading to deviations in the dispersion coefficient beyond the effects of rock heterogeneity alone. In more homogeneous media, a threshold is observed where dispersion under unstable flow is lower relative to stable flow. These findings demonstrate that pressure amplifies dispersion primarily under unstable flow governed by the fluid density contrasts, and that heterogeneity can either enhance or dampen these effects.

1. Introduction

The mixing of fluids in porous media plays a critical role in subsurface flow and transport processes, influencing applications such as geological carbon or hydrogen storage, enhanced gas recovery, and contaminant transport [1,2]. Physical dispersion is governed by two primary mechanisms: mechanical dispersion and molecular diffusion [3]. Mechanical dispersion arises from variations in pore sizes and flow pathways, causing velocity differences that stretch the fluid front and enhance mixing. This effect becomes more significant at higher flow velocities, where velocity contrasts amplify fluid spreading [4,5]. In contrast, molecular diffusion is constrained by tortuous pore geometries, which can either enhance or impede transport [6–8]. At high flow velocities, mechanical dispersion dominates, whereas at low velocities, diffusion plays a more significant role in smoothing concentration gradients, leading to a composite dispersion behavior.

System pressure influences dispersion by altering fluid properties such as density, viscosity, and compressibility, which in turn affect velocity distributions and flow stability. Pressure-dependent changes in gas viscosity impact the relative contributions of advective transport and molecular diffusion. At lower pressures, reduced fluid density can suppress small-scale instabilities, leading to more stable flow regimes where dispersion is primarily controlled by pore-scale heterogeneity [9,10]. This stabilization effect decreases velocity contrasts and may lower the dispersion coefficient. In contrast, under unstable flow conditions, increasing pressure can intensify velocity fluctuations, resulting in more chaotic mixing and an elevated dispersion coefficient beyond the effects of heterogeneity alone.

The influence of pressure also depends on the heterogeneity of the medium [11]. In relatively homogeneous rocks, where pores and throats are more uniform, lowering the system pressure would reduce velocity differentials across pores. This occurs because compressibility effects are minimized and the velocity field becomes smoother, resulting in a narrower distribution of flow pathways. Since there are fewer velocity contrasts to stretch and mix the solute front, dispersion decreases. In contrast, highly heterogeneous formations, characterized by wide

* Corresponding author.
E-mail address: quoc_p_nguyen@mail.utexas.edu (Q.P. Nguyen).

https://doi.org/10.1016/j.jcou.2026.103467
Received 7 January 2026; Received in revised form 10 April 2026; Accepted 18 May 2026
Available online 21 May 2026

variations in pore size, throat size, and connectivity, respond differently to pressure. At elevated pressures, density and viscosity contrasts between displacing and displaced gases become more pronounced. These contrasts amplify local velocity fluctuations, which interact with the heterogeneous pore structure to generate more complex pathways. These mechanisms are particularly relevant for gas storage operations that rely on injection and production from the same well, where alternating flow directions can repeatedly disrupt established concentration profiles and promote enhanced mixing. Such cycling can alter dispersion, particularly near the wellbore where flow rate is much higher than that in the far field region, which would impact storage efficiency, gas recovery, and the predictability of breakthrough times.

The role of pore structure has also been examined in recent works using advanced imaging techniques and pore-network modeling. High-resolution micro-CT studies have shown that pore coordination number, aspect ratio, and connectivity strongly influence local velocity distribution and therefore mechanical dispersion [12,13]. These studies suggest that even subtle differences in pore geometry can induce significant variations in mixing behavior, especially under dynamic gas storage conditions. OpenPNM and lattice-Boltzmann-based models have been widely employed to capture these effects, providing insights into the coupling between pore-scale architecture and macroscopic transport properties [14–16]. Emerging research is also exploring the coupling between dispersion and geochemical processes, such as the dissolution of CO_2 into formation brine or the adsorption of gases in organic-rich formations. These reactive transport effects can feed back into the flow field by altering fluid properties and pore structure, which would influence dispersion behavior over time [17,18]. Such couplings are especially relevant for long-term CO_2 storage scenarios, where both chemical and mechanical effects evolve concurrently.

In addition to the influence of flow velocity and heterogeneity, several studies have demonstrated the role of thermophysical properties of gases and pore-scale processes in controlling mixing in porous media. For instance, the compressibility and the phase portioning of the injected gas can alter local pressure gradients and flow paths, which in turn affect both the longitudinal and transverse components of dispersion [19–21]. This is particularly critical for underground gas storage, where cyclic injection and withdrawal lead to repeated non-equilibrium conditions and complex flow patterns [19,20]. Gas compressibility and real gas effects are of growing interest because they influence the transition between diffusion- and advection-dominated mass transfer regimes. For non-ideal gas mixtures such as CO_2–CH_4 or H_2–CO_2, compositional effects introduce additional complexity, as species-dependent diffusion coefficients and variable density gradients create differential migration and non-Fickian diffusion [22–24]. This non-Fickian behavior occurs when multi-component interactions cause fluid mixing to deviate from the proportional relationship between component mass flux and concentration gradient [23]. This leads to the development of localized concentration fronts and preferential channels that are not predicted by classical dispersion models. Nazari et al. investigated the dispersion behavior of non-ideal binary gas mixtures during underground hydrogen storage (UHS). Numerical modeling, supported by experimental validation, shows that dispersivity during gas injection and production is influenced not only by the properties of the porous medium but also significantly by gas-specific thermodynamic factors such as compressibility and diffusivity. Unlike Newtonian fluids, gases exhibited non-unique dispersion coefficients that vary between injection and production, particularly in systems with high non-ideality such as H_2–CO_2. To account for this, a gas-specific correction factor for dispersivity was introduced based on a strong correlation with the compressibility factor ratio of advancing and receding gases.

While previous research has examined dispersion under different flow rates and rock heterogeneities, the effect of system pressure on dispersion remains less understood. Previous studies have primarily focused on how pressure influences permeability, relative permeability, and multiphase flow behavior in porous media, but its role in modifying dispersion dynamics and flow stability has received limited attention [10–14]. Particularly the extent to which pressure stabilizes or destabilizes flow, and its impact on fluid mixing, has not been systematically explored. This study addresses these gaps by investigating the effects of pressure and flow rate on gas dispersion in Indiana limestone and Silurian dolomite using CO_2 and CH_4 as the working gases. CO_2 and CH_4 have distinct physical properties, including differences in density and viscosity, which influence their dispersion behavior under varying flow and pressure conditions. Experiments were conducted at pressures of 300, 600, and 900 psi with flow rates of 1.69×10^{-4} m/s, 2.12×10^{-4} m/s, and 3.39×10^{-4} m/s to assess how dispersion characteristics change under different conditions.to assess how dispersion characteristics change under different conditions.

2. Background

2.1. Longitudinal dispersion coefficient

The dispersion process can be described by the 1-dimensional advective–dispersion equation [15]. This equation accounts for both the advection of a chemical species (referred to as a solute) by the fluid flow and its diffusion due to concentration gradients:

$$\frac{\partial C}{\partial t} + u\frac{\partial C}{\partial x} = K_L\frac{\partial^2 C}{\partial x^2} \quad , \tag{1}$$

$$u = \frac{Q}{A\phi} \quad , \tag{2}$$

where C is the concentration of the solute, $u\left(\frac{m}{s}\right)$ is the interstitial velocity, $t(s)$ is the time, Q $\left(\frac{m^3}{s}\right)$ is the volumetric flow rate, A (m^2) is the cross-sectional area perpendicular to the flow direction, and ϕ is the porosity of the porous medium. The dispersion coefficient K_L is expressed by Eq. 3, where $D_e\left(\frac{m^2}{s}\right)$ is the molecular diffusivity, $\alpha\,(m)$ is the dispersivity, and n is the exponent [2].

$$K_L = D_e + \alpha u^n \tag{3}$$

The molecular diffusivity is a function of pressure, while the dispersivity quantifies the extent of mechanical dispersion due to variations in fluid velocity within pore spaces [2]. In this work, K_L was determined by first fitting the observed concentration profiles obtained from the core-flooding experiments to the solution of the 1D advection-diffusion (Eq. 3) to determine Peclet number [16,17].

$$C_D = \frac{1}{2}\left[\operatorname{erfc}\left(\frac{x_D - t_D}{2\left(\frac{t_D}{P_e}\right)^{\frac{1}{2}}}\right)\right] + \frac{1}{2}\exp(x_D P_e)\left[\operatorname{erfc}\left(\frac{x_D + t_D}{2\left(\frac{t_D}{P_e}\right)^{\frac{1}{2}}}\right)\right] \quad , \tag{4}$$

where $C_0\left(\frac{mol}{m^3}\right)$ is the inlet concentration, C is the concentration at the given time at the outlet, C_D is the dimensionless concentration defined as the ratio of C to C_0. $L(m)$ is the characteristic length of the porous medium, P_e is the experimental Peclet number, $x_D = x/L$ is the dimensionless length, $t_D = ut/L$ is the dimensionless time. The Peclet number is used to calculate the longitudinal dispersion coefficient according to Eq. 4.

$$K_L = \frac{uL}{P_e} \tag{5}$$

2.2. Flow stability

Flow stability is particularly relevant, as instabilities can enhance mixing and dispersion beyond what is predicted by classical Fickian models [6,18,19]. Flow instabilities occur when perturbations in velocity fields are amplified due to rock heterogeneity or unfavorable viscosity and density contrasts. These instabilities can lead to preferential flow pathways, bypassing certain regions while enhancing mixing in others. One of the fundamental descriptions of fluid instability in porous media is given by the Saffman-Taylor instability, which occurs when a less viscous fluid displaces a more viscous fluid in a porous medium [20]. This instability leads to the formation of finger-like patterns at the interface, enhancing mixing and dispersion beyond what would be expected from molecular diffusion and mechanical dispersion alone. In a steady-state system with a vertical upward velocity u and a horizontal interface between the two fluids, the interface remains stable for small deviations from the steady state if:

$$\left(\frac{\mu_2}{k_2}-\frac{\mu_1}{k_1}\right)u+(\rho_2-\rho_1)g>0, \tag{4}$$

and unstable if:

$$\left(\frac{\mu_2}{k_2}-\frac{\mu_1}{k_1}\right)u+(\rho_2-\rho_1)g<0, \tag{5}$$

where the suffix 1 refers to the displaced fluid and suffix 2 refers to the displacing fluids. Additionally, $\mu\ (Pa\bullet s)$ is the fluid viscosity, $k(m^2)$ is the permeability, $\rho\left(\frac{kg}{m^3}\right)$ is the fluid density, and $g(\frac{m^2}{s})$ is the acceleration due to gravity. The viscosity and the density of CO_2 is always higher than that of CH_4 at the pressures and temperature evaluated in this work. Hence, the system is considered stable when CO_2 displaces CH_4, while it is deemed unstable when CH_4 displaces CO_2. A summary of the calculation performed for flow stability is shown in Table A5 in the Appendix.

3. Experiments

This section describes the gas dispersion experiments, including the materials, the core-flooding apparatus, and the experimental procedure. The materials section details the rock samples and gases used in the study. The apparatus section covers the core-flooding setup, including instrumentation for pressure regulation, flow control, and effluent analysis. The procedure details the experimental workflow, from sample preparation to data collection and processing. Section 3 presents the analysis of results, followed by discussion of the findings in Section 4.

3.1. Materials

The experiments were conducted on two carbonate rock samples that were selected for their distinct pore structure while retaining the same porosity and permeability. These cores were prepared into cylindrical samples with a diameter of 0.0254 m and a length of 0.3048 m, detailed in Table 1. The working gases, CO_2 and CH_4, were supplied by Praxair. The methane was ultra-high purity with a mole fraction of 0.99995, while the liquid CO_2 had a mole fraction purity greater than 0.999. To ensure gas was the only phase present, the core samples were thoroughly dried before testing to eliminate any residual moisture that could affect gas flow. Additionally, prior to each experiment, the rock samples were vacuum-dried and saturated with CH_4 up to the targeted experimental pressure (300, 600, 900 psi) to establish initial conditions.

Table 1
A summary of core samples used in this study.

Rock Type	Porosity (%)	Brine permeability (md)	Brine permeability (m^2)	Diameter (m)	Length (m)
ILS	15	5.5	5.43×10^{-15}	0.0254	0.3048
SD	15	5.1	5.03×10^{-15}	0.0254	0.3048

3.2. Apparatus and procedure

The gas dispersion experiments were conducted using a controlled core-flooding setup to investigate the effects of pressure, flow stability, and rock heterogeneity on dispersion, shown in Fig. 1. The experimental procedure began with core preparation, where the rock samples were dried in an oven at 100°C for at least 24 h to remove any residual moisture, ensuring that the only phase present during the experiment was gas. The dried core was then placed inside a flexible rubber sleeve within the core holder, and confining oil was pressurized to 100 psi above the system pressure to prevent bypass flow. Before gas injection, the core was vacuumed for one hour to remove any remaining gases. Once prepared, ultra-high purity CH_4 was injected into the core at the target system pressure (300, 600, or 900 psi) to fully saturate the pore space. Following saturation, CO_2 was introduced at a controlled rate (1.69×10^{-4} m/s, 2.12×10^{-4} m/s, and 3.39×10^{-4} m/s) at 65 °C and the target system pressure) using a high-precision Quizix pump to displace CH_4. Pressure gauges at the inlet and outlet continuously monitored pressure variations and the pressure drop across the core. Effluent gas samples were collected and analyzed using a gas chromatograph to determine CH_4 and CO_2 concentrations over time. Note that the repeatability of the coreflood experiments is high with a relative standard deviation (RSD) is about 1.8%. This deviation was determined based on 3 repetitions of a CO_2 displacing methane experiment at 900 psi and 65 °C. Moreover, the overall measurement accuracy of the GC instrument used in this work evaluated through independent recovery studies was within the 98–102% range. These repeatability and accuracy were used to estimate the experimental errors shown in the figures in the Results and Discussion.

3.3. Data processing

The analysis of physical dispersion in rock samples requires data processing to extract transport parameters from gas chromatography measurements. First, the effluent from the core-flooding experiments were analyzed using gas chromatography (GC) to determine CO_2 and CH_4 concentrations over time. The measured concentrations were then plotted against injected pore volumes to generate an elution curve. To quantify dispersion, the experimental elution curve was fitted to the one-dimensional (1D) advection-dispersion equation (Eq. 3), allowing for the determination of the experimental Peclet number. Finally, the longitudinal dispersion coefficient was calculated using the fitted Peclet number, as described in Eq. 4.

4. Results

4.1. The effect of pressure on dispersion

Fig. 2 shows the elution curves for Indiana limestone at an injection rate of 2.12×10^{-4} m/s under system pressures of 300, 600, and 900 psi. For the same pore structure and injection rate, the curves overlapped. This suggests that under stable flow conditions, the transport of gases through the porous medium remains unaffected by pressure variations.

Additionally, the overlap in breakthrough profiles across different pressures implies that dispersion is primarily controlled by pore structure rather than compressibility or viscosity changes at stable flow conditions. At a given injection rate, the velocity field within the rock remained unchanged across different pressures, which led to consistent advective transport and mechanical dispersion characteristics. Since both CO_2 and CH_4 exhibit relatively low viscosities and similar diffusion properties under stable flow, pressure-induced changes in molecular diffusion and velocity gradients are to be minimal.

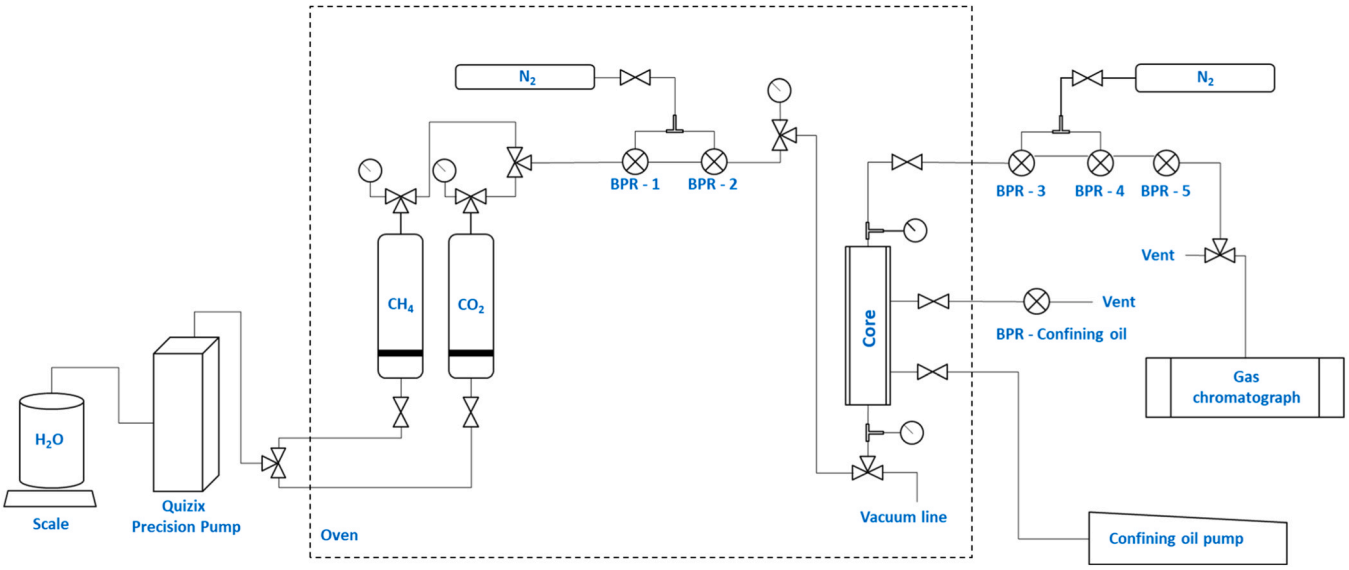

Fig. 1. Experimental apparatus and its components.

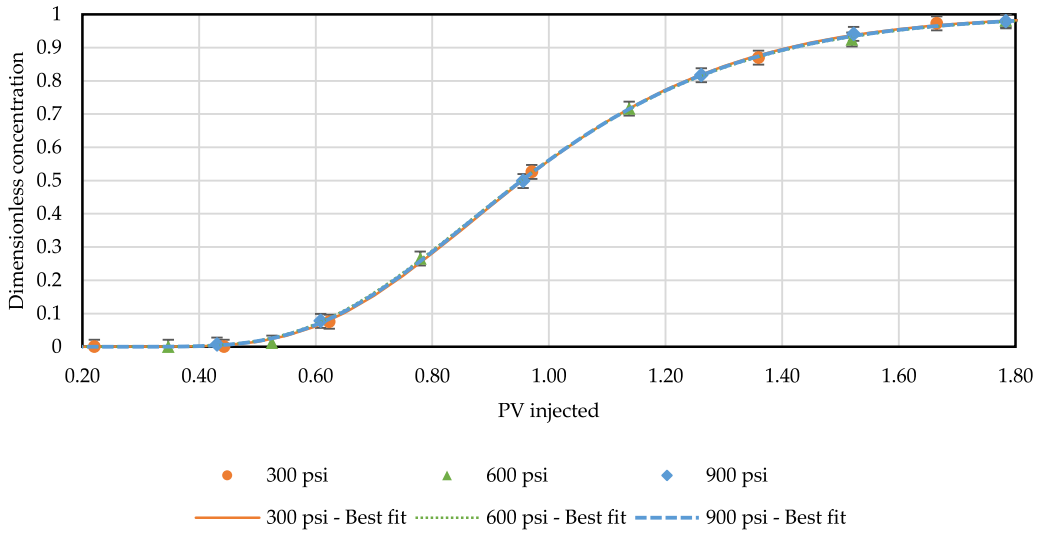

Fig. 2. Pressure effect on Indiana limestone at a rate of 2.12×10^{-4} m/s (CO_2 displacing CH_4).

4.2. *Flow stability*

Variations in system pressure influence fluid properties such as density and viscosity, thereby affecting the balance between advective transport and dispersion. Figs. 4 and 5 present the elution curves for CO_2 displacing CH_4 at an injection rate of 3.39×10^{-4} m/s under system pressures of 300 and 900 psi. At 300 psi, the elution curve for the unstable flow was steeper than that of the stable flow, indicating reduced dispersion. This suggests that at lower pressures, flow instabilities restricted transverse mixing and confined the displacement front. Moreover, the combined effects of rock heterogeneity and lower pressure may have dampened instability-driven fluctuations. In contrast, at 900 psi, the elution curve for the unstable flow was broader than that of the stable flow, indicating enhanced dispersion. This suggests that flow instabilities promoted mixing by increasing local velocity variation and sensitivity to rock heterogeneity.

5. Discussion

5.1. *Effect of pressure on flow stability and dispersion*

Fig. 6 presents the dispersion coefficient as a function of interstitial velocity for system pressures of 300, 600, and 900 psi in Indiana Limestone, with values summarized in Tables A1–A2 in the Appendix. In scenarios where CH_4 is displacing CO_2, higher pressures would enhance instability-driven mixing. However, when CO_2 is displacing CH_4, dispersion remains largely unaffected, aside from a minor reduction due to decreased diffusivity. A distinct crossover point is observed where the dispersion coefficient for unstable flow intersects that of stable flow, with the velocity at this intersection decreasing as system pressure increases. Additionally, for unstable flow, the slope of the dispersion coefficient curve increases with pressure, indicating a stronger dependence on velocity.

For stable flow, the dispersion coefficient decreases slightly with increasing pressure, and the slope of the stable flow curve remains unchanged. This trend may be attributed to reduced molecular diffusivity at higher pressures, which limits diffusion's contribution to overall

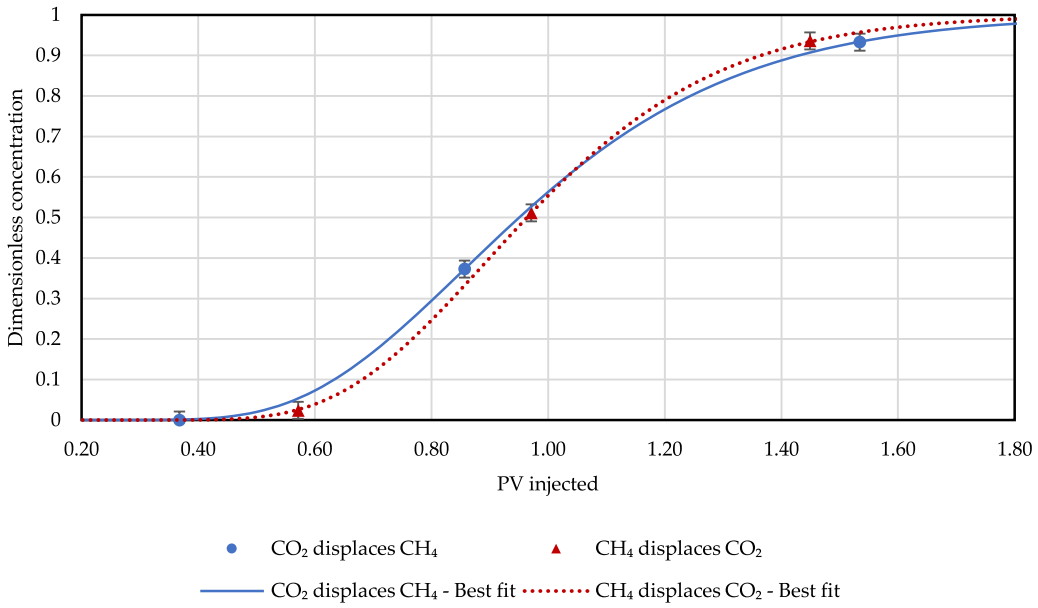

Fig. 4. Flow stability effect on Indiana limestone at a rate of 3.39 × 10^{-4} m/s and 300 psi.

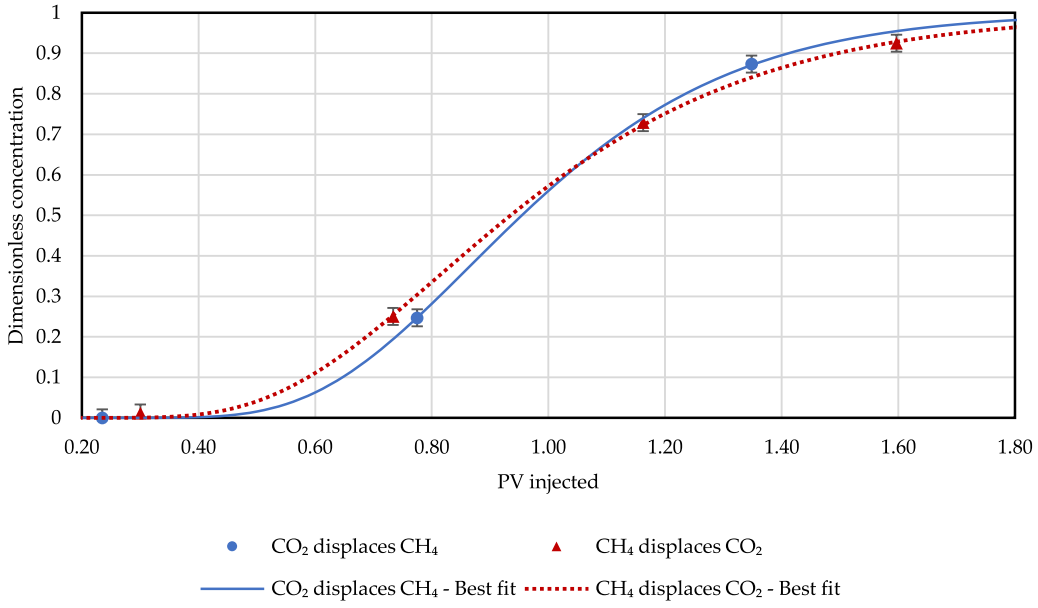

Fig. 5. Flow stability effect on Indiana limestone at a rate of 3.39 × 10^{-4} m/s and 900 psi.

dispersion [21]. Since stable flow is primarily governed by advective transport and rock heterogeneity rather than instability-driven mixing, the impact of pressure on dispersion remains minimal.

At lower pressures, the unstable flow curve lies below the stable flow curve, suggesting reduced dispersion in the unstable regime. This may result from the formation of preferential flow channels, where CH_4 advances through high-permeability pathways within the CO_2 phase, limiting mixing [22]. In such cases, instability does not enhance dispersion but instead localizes flow into distinct pathways. As pressure increases, these effects diminish, and instability-driven mixing becomes the dominant mechanism controlling dispersion. Higher pressures amplify density and viscosity contrasts between CH_4 and CO_2, increasing velocity fluctuations from flow instabilities. This leads to broader dispersion profiles, as unstable flow promotes more extensive mixing compared to lower-pressure conditions.

5.2. *Impact of heterogeneity on flow stability and dispersion*

Silurian dolomite is widely recognized as more heterogeneous than Indiana limestone, with broader pore-size distributions and more irregular pore-throat connectivity. MICP and water NMR analyses performed in previous studies confirm that dolomite exhibits a wider range of pore throat sizes than the relatively uniform network of Indiana limestone, producing stronger velocity contrasts and greater mechanical dispersion [26,27]. By contrast, Indiana limestone is relatively homogeneous, with only modest millimeter-scale variability [28]. These differences explain why pressure-dependent instabilities strongly affect dispersion in Indiana limestone but contribute little additional effect in Silurian dolomite.

Fig. 7 presents the dispersion coefficient as a function of interstitial velocity for both rocks under stable flow, where CO_2 displaces CH_4. The values are also summarized in the Appendix. In both rocks, dispersion

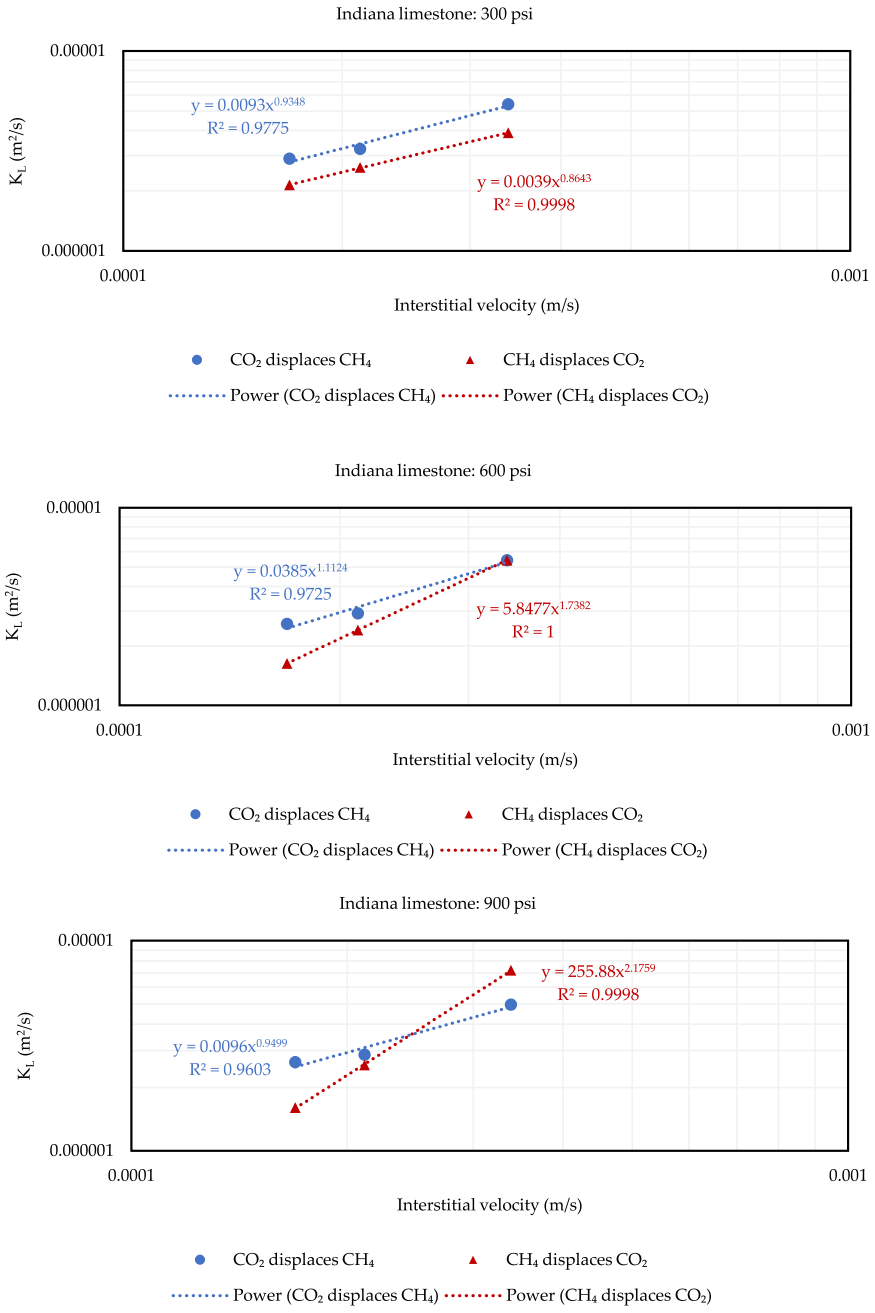

Fig. 6. Dispersion coefficient vs interstitial velocity for 300 psi, 600 psi and 900 psi in Indiana Limestone.

coefficients change only slightly with increasing pressure, reflecting the limited influence of pressure under stable flow. For Silurian dolomite, in particular, advective transport pathways are controlled mainly by pore connectivity rather than compressibility effects. As a result, increasing pressure reduces dispersion only marginally by lowering molecular diffusivity, while the overall dispersion–velocity relationship remains essentially unchanged.

Fig. 8 shows the dispersion coefficient plotted against interstitial velocity for Indiana limestone and Silurian dolomite under unstable flow conditions, where the effect of rock heterogeneity becomes even more evident. In this flow regime, both the trend and magnitude of the dispersion coefficient as shown in Fig. 8 vary with velocity and system pressure. While pressure-dependent instabilities significantly enhance dispersion in Indiana limestone (i.e. increase of KL value with pressure at the highest velocity, Fig. 8-Indiana limestone), this effect is much less evident in Silurian dolomite because of its greater heterogeneity (i.e. KL does not significantly increase with pressure at the highest velocity, Fig. 8-Silurian dolomite). In the limestone, which is relatively homogeneous, changes in pressure alter density and viscosity contrasts between CO_2 and CH_4, which amplified velocity fluctuations. This produced a clear separation between dispersion–velocity curves at different pressures (Fig. 8-Indiana limestone). In contrast, Silurian dolomite exhibits a broad distribution of pore and throat sizes, irregular connectivity, and more complex flow pathways. As a result, additional pressure-driven instabilities have little effect, and the dispersion-velocity curves at 300, 600, and 900 psi nearly overlap (Fig. 8–Silurian dolomite). This indicates that in highly heterogeneous formations, dispersion is governed primarily by mechanical spreading imposed by pore structure, whereas in more homogeneous rocks, pressure-driven instabilities play a greater role in enhancing mixing.

While this study provides insights into the effects of system pressure, flow stability, and rock heterogeneity on gas dispersion in carbonate

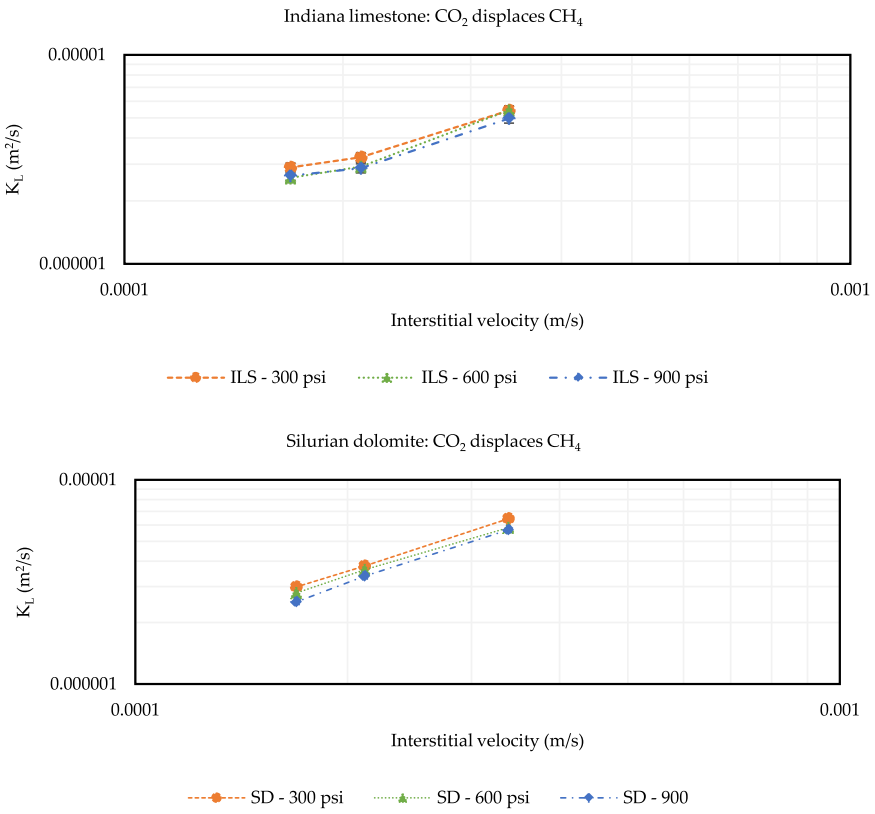

Fig. 7. K_L vs. average interstitial velocity for Indiana limestone and Silurian dolomite at 300, 600, and 900 psi, where CO_2 displaces CH_4.

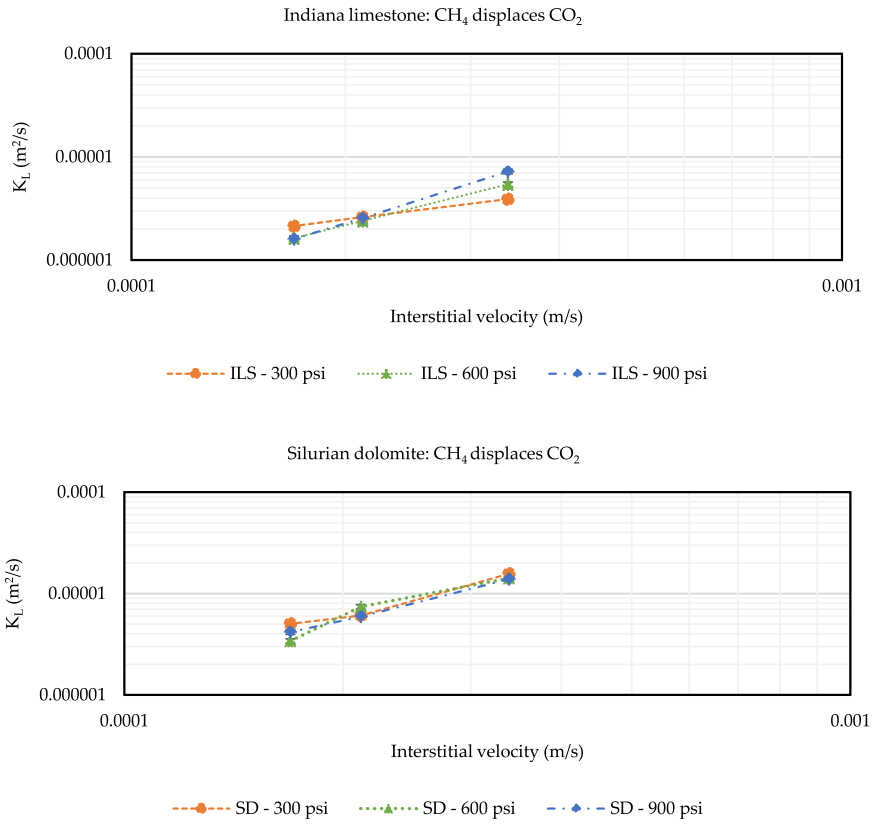

Fig. 8. K_L vs. average interstitial velocity for Silurian dolomite at 300, 600, and 900 psi.

formations, several limitations remain. First, the analysis was limited to Indiana limestone and Silurian dolomite, which do not fully capture the diversity of all carbonate structures. Carbonates with fractures may influence dispersion differently [23–28]. Second, this study relied on elution curves and longitudinal dispersion coefficients to characterize gas transport, which provide macroscopic insights but do not resolve pore-scale mechanisms. The observed trends suggest a complex relationship between pore structure, instability, and flow regime, but a systematic investigation of pore connectivity, coordination number, and pore-throat size distribution remains necessary.

High-resolution imaging techniques, such as X-ray micro-computed tomography (micro-CT) combined with pore-scale simulations, could better quantify how pore structure influences dispersion under varying flow conditions. Future work will focus on isolating pore structure parameters to establish quantitative relationships and develop a scaling law that links pore-scale to core-scale dispersion mechanisms, and aids in upscaling these mechanisms to field.

6. Conclusions

This study examined the effects of system pressure, flow stability, and rock heterogeneity on gas dispersion in carbonate formations using CO_2 and CH_4. Elution curves and longitudinal dispersion coefficients were analyzed for Indiana limestone and Silurian dolomite under stable and unstable flow regimes at varying pressures and injection rates. The influence of system pressure on dispersion depends on flow stability. Under stable flow, pressure had little effect, suggesting that transport was primarily controlled by pore structure. Additionally, higher pressures slightly reduced the dispersion coefficient due to lower molecular diffusivity. In contrast, under unstable flow, system pressure had a more pronounced impact. At lower pressures, instability-driven mixing was suppressed, causing CH_4 to displace CO_2 through preferential pathways, thereby limiting dispersion. However, at higher pressures, greater density and viscosity contrasts intensified velocity fluctuations, enhancing mixing driven by flow instabilities.

While pressure had little effect on dispersion in stable flow regimes, it became significant under unstable conditions, which also varied with rock heterogeneity. In stable flow, Silurian dolomite exhibited a higher dispersion coefficient at lower pressures, suggesting that its complex pore structure enhanced mixing. Under unstable conditions, heterogeneity suppressed pressure-dependent instability effects, resulting in nearly the same relationship between dispersion coefficient and interstitial velocity for all pressures studied in the present work. This indicates a complex relationship between system pressure, injection rate, and rock heterogeneity, where mechanical dispersion in highly heterogeneous rocks moderates the effects of pressure-driven instability.

CRediT authorship contribution statement

Rouhi Farajzadeh: Writing – review & editing, Project administration, Methodology, Investigation, Formal analysis, Conceptualization. **Quoc P. Nguyen:** Writing – review & editing, Validation, Supervision, Resources, Methodology, Investigation, Funding acquisition, Formal analysis, Data curation, Conceptualization. **Tri Pham:** Writing – original draft, Validation, Methodology, Investigation, Formal analysis, Data curation, Conceptualization.

Declaration of Competing Interest

The authors declare that they have no known competing financial interests or personal relationships that could have appeared to influence the work reported in this paper.

Acknowledgements

The authors thank Sahar Hoornahad from Shell for reviewing initial draft of this submission. Authors also thank Shell Global Solutions International B.V. for granting permission to publish this work.

Appendix A

Table A1
Longitudinal dispersion coefficient for Indiana limestone 300, 600, and 900 psi at stable flow condition

Interstitial velocity (m/s)	K_L (m^2/s) at P = 300 psi	K_L (m^2/s) at P = 600 psi	K_L (m^2/s) at P = 900 psi
1.69×10^{-4}	2.89×10^{-6}	2.58×10^{-6}	2.64×10^{-6}
2.12×10^{-4}	3.24×10^{-6}	2.92×10^{-6}	2.87×10^{-6}
3.39×10^{-4}	5.42×10^{-6}	5.43×10^{-6}	4.96×10^{-6}

Table A2
Longitudinal dispersion coefficient for Indiana Limestone for 300, 600, and 900 psi at unstable flow condition

Interstitial velocity (m/s)	K_L (m^2/s) at P = 300 psi	K_L (m^2/s) at P = 600 psi	K_L (m^2/s) at P = 900 psi
1.69×10^{-4}	2.14×10^{-6}	1.63×10^{-6}	1.60×10^{-6}
2.12×10^{-4}	2.61×10^{-6}	2.40×10^{-6}	2.56×10^{-6}
3.39×10^{-4}	3.90×10^{-6}	5.43×10^{-6}	7.22×10^{-6}

Table A3
Longitudinal dispersion coefficient for Silurian Dolomite for 300, 600, and 900 psi at stable flow condition

Interstitial velocity (m/s)	K_L (m^2/s) at P = 300 psi	K_L (m^2/s) at P = 600 psi	K_L (m^2/s) at P = 900 psi
1.69×10^{-4}	2.99×10^{-6}	2.79×10^{-6}	2.52×10^{-6}
2.12×10^{-4}	3.79×10^{-6}	3.63×10^{-6}	3.37×10^{-6}
3.39×10^{-4}	6.46×10^{-6}	5.83×10^{-6}	5.69×10^{-6}

Table A4
Longitudinal dispersion coefficient for Silurian Dolomite for 300, 600, and 900 psi at unstable flow condition

Interstitial velocity (m/s)	K_L (m^2/s) at P = 300 psi	K_L (m^2/s) at P = 600 psi	K_L (m^2/s) at P = 900 psi
1.69×10^{-4}	5.03×10^{-6}	3.40×10^{-6}	4.16×10^{-6}
2.12×10^{-4}	6.06×10^{-6}	7.40×10^{-6}	5.92×10^{-6}
3.39×10^{-4}	1.57×10^{-5}	1.42×10^{-5}	1.38×10^{-5}

Table A5
Calculation of flow stability conditions from Eq. 5

Pressure	CO_2 density (kg/m^3)	CH_4 density (kg/m^3)	CO_2 viscosity (Pa•s)	CH_4 viscosity (Pa•s)	Interstitial velocity (m/s)	Stable flow (CO_2 displaces CH_4)	Unstable flow (CH_4 displaces CO_2)
300	3.49×10^{1}	1.21×10^{1}	1.71×10^{-5}	1.27×10^{-5}	1.69×10^{-4}	1.51×10^{5}	-1.51×10^{5}
					2.12×10^{-4}	1.89×10^{5}	-1.89×10^{5}
					3.39×10^{-4}	3.02×10^{5}	-3.02×10^{5}
600	7.62×10^{1}	2.46×10^{1}	1.75×10^{-5}	1.31×10^{-5}	1.69×10^{-4}	1.53×10^{5}	-1.53×10^{5}
					2.12×10^{-4}	1.92×10^{5}	-1.92×10^{5}
					3.39×10^{-4}	3.07×10^{5}	-3.07×10^{5}
900	1.27×10^{2}	3.77×10^{1}	1.85×10^{-5}	1.35×10^{-5}	1.69×10^{-4}	1.70×10^{5}	-1.70×10^{5}
					2.12×10^{-4}	2.14×10^{5}	-2.14×10^{5}
					3.39×10^{-4}	3.41×10^{5}	-3.41×10^{5}

Data Availability

Data will be made available on request.

References

[1] P. de Anna, T. Le Borgne, M. Dentz, A.M. Tartakovsky, D. Bolster, P. Davy, Flow intermittency, dispersion, and correlated continuous time random walks in porous media, Phys. Rev. Lett. 110 (2013) 184502, https://doi.org/10.1103/PhysRevLett.110.184502.

[2] J. Bear, Dynamics of fluids in porous media, J. Fluid Mech. 61 (1973) 206–208, https://doi.org/10.1017/S0022112073210662.

[3] R. Mao, X. Luo, J.J. Jiao, H. Li, Molecular diffusion and pore-scale mechanical dispersion controls on time-variant travel time distribution in hillslope aquifers, J. Hydrol. (Amst.) 616 (2023) 128798, https://doi.org/10.1016/j.jhydrol.2022.128798.

[4] Z. Wang, K. Chauhan, J.-M. Pereira, Y. Gan, Disorder characterization of porous media and its effect on fluid displacement, Phys. Rev. Fluids 4 (2019) 034305, https://doi.org/10.1103/PhysRevFluids.4.034305.

[5] A. Puyguiraud, P. Gouze, M. Dentz, Pore-scale mixing and the evolution of hydrodynamic dispersion in porous media, Phys. Rev. Lett. 126 (2021) 164501, https://doi.org/10.1103/PhysRevLett.126.164501.

[6] B. Bijeljic, P. Mostaghimi, M.J. Blunt, Signature of non-fickian solute transport in complex heterogeneous porous media, Phys. Rev. Lett. 107 (2011) 204502, https://doi.org/10.1103/PhysRevLett.107.204502.

[7] A. Fick, On liquid diffusion, Lond. Edinb. Dublin Philos. Mag. J. Sci. (1855).

[8] T.K. Perkins, O.C. Johnston, A review of diffusion and dispersion in Porous Media, Soc. Pet. Eng. J. 3 (1963) 70–84, https://doi.org/10.2118/480-PA.

[9] T. Menand, A.W. Woods, Dispersion, scale, and time dependence of mixing zones under gravitationally stable and unstable displacements in porous media, Water Resour. Res 41 (2005), https://doi.org/10.1029/2004WR003701.

[10] J. Chen, G. Wang, J. Yang, T. Lei, K.H. Luo, Pore-scale study of miscible density instability with viscosity contrast in porous media, Phys. Fluids 35 (2023), https://doi.org/10.1063/5.0161872.

[11] D.W. Vasco, S.E. Minkoff, Modelling flow in a pressure-sensitive, heterogeneous medium, Geophys J. Int 179 (2009) 972–989, https://doi.org/10.1111/j.1365-246X.2009.04330.x.

[12] X. Qin, Y. Xia, J. Qiao, J. Chen, J. Zeng, J. Cai, Modeling of multiphase flow in low permeability porous media: effect of wettability and pore structure properties, J. Rock. Mech. Geotech. Eng. 16 (2024) 1127–1139, https://doi.org/10.1016/j.jrmge.2023.06.007.

[13] S. Bekri, P.M. Adler, Dispersion in multiphase flow through porous media, Int. J. Multiph. Flow. 28 (2002) 665–697, https://doi.org/10.1016/S0301-9322(01)00089-1.

[14] F.J. Carrillo, I.C. Bourg, C. Soulaine, Multiphase flow modeling in multiscale porous media: an open-source micro-continuum approach, J. Comput. Phys. X 8 (2020) 100073, https://doi.org/10.1016/j.jcpx.2020.100073.

[15] G. Taylor, Dispersion of soluble matter in solvent flowing slowly through a tube, Proc. R. Soc. Lond. A Math. Phys. Sci. 219 (1953) 186–203, https://doi.org/10.1098/rspa.1953.0139.

[16] J.J. Fried, M.A. Combarnous, Dispers. Porous Media (1971) 169–282, https://doi.org/10.1016/B978-0-12-021807-3.50008-4.

[17] W.E. Brigham, Mixing equations in short laboratory cores, Soc. Pet. Eng. J. 14 (1974) 91–99, https://doi.org/10.2118/4256-PA.

[18] L.W. Gelhar, C. Welty, K.R. Rehfeldt, A critical review of data on field-scale dispersion in aquifers, Water Resour. Res. 28 (1992) 1955–1974, https://doi.org/10.1029/92WR00607.

[19] B. Bijeljic, A. Raeini, P. Mostaghimi, M.J. Blunt, Predictions of non-Fickian solute transport in different classes of porous media using direct simulation on pore-scale images, Phys. Rev. E 87 (2013) 013011, https://doi.org/10.1103/PhysRevE.87.013011.

[20] P. Saffman, G. Taylor, The penetration of a fluid into a porous medium or Hele-Shaw cell containing a more viscous liquid, Proc. R. Soc. Lond. A Math. Phys. Sci. 245 (1958) 312–329, https://doi.org/10.1098/rspa.1958.0085.

[21] S. Takahashi, The diffusion of gases at high pressures. V. The diffusion of CTH3 in the CO2–Ar System, Bull. Chem. Soc. Jpn 47 (1974) 1342–1345, https://doi.org/10.1246/bcsj.47.1342.

[22] Z. Chen, L. Li, Y. Su, J. Liu, Y. Hao, X. Zhang, Investigation of CO2-EOR and storage mechanism in Injection-Production coupling technology considering reservoir heterogeneity, Fuel 368 (2024) 131595, https://doi.org/10.1016/j.fuel.2024.131595.

[23] C. Zhang, K. Zhang, J. Mo, Z. Li, T. Suekane, Y. Wang, M. Li, Pore-scale investigation of solute dispersion behavior in porous media under a two-phase co-flow condition, Adv. Water Resour. 186 (2024) 104664, https://doi.org/10.1016/j.advwatres.2024.104664.
[24] D.B. Grove, W.A. Beetem, Porosity and dispersion constant calculations for a fractured carbonate aquifer using the two well tracer method, Water Resour. Res 7 (1971) 128–134, https://doi.org/10.1029/WR007i001p00128.
[25] Q. Ding, J. Wang, L. Yang, D. Zhu, W. Jiang, Z. He, Exploring the role of the structural heterogeneity of fractured carbonate reservoirs in contact with dissolved CO2 based on fracture-water-rock simulation experiments, Appl. Geochem. 150 (2023) 105589, https://doi.org/10.1016/j.apgeochem.2023.105589.
[26] H. Sun, S. Vega, G. Tao, Analysis of heterogeneity and permeability anisotropy in carbonate rock samples using digital rock physics, J. Pet. Sci. Eng. 156 (2017) 419–429, https://doi.org/10.1016/j.petrol.2017.06.002.
[27] D.B. Grove, W.A. Beetem, Porosity and dispersion constant calculations for a fractured carbonate aquifer using the two well tracer method, Water Resour. Res. 7 (1971) 128–134.
[28] Q. Ding, J. Wang, L. Yang, D. Zhu, W. Jiang, Z. He, Exploring the role of the structural heterogeneity of fractured carbonate reservoirs in contact with dissolved CO_2 based on fracture-water-rock simulation experiments, Appl. Geochem 150 (2023) 105589.